# Electronic Supplementary Information

## Zero-Dimensional Hybrid Binuclear Manganese Chloride with Thermally Stable Yellow Emission

Liming Zhang[‡,a,b], Zhishan Luo[‡,b,] Yi Wei[b], Wei Wang[b], Yulian Liu[b], Chen Li[b], Xin He[b], Zewei Quan[b]*

[a] School of Chemistry and Chemical Engineering, Harbin Institute of Technology (HIT), Harbin, 150001, China.

[b] Department of Chemistry and Academy for Advanced Interdisciplinary Studies, Southern University of Science and Technology (SUSTech), Shenzhen, 518055, China.

[‡] These authors contribute equally to this work.

* Corresponding author

## Experimental Procedures

### Materials
Manganese (II) chloride ($MnCl_2$, 95%), lead (II) chloride ($PbCl_2$, 98%), 1,4,7,10,13,16-hexaoxacyclooctadecane (18-crown-6, 99%), acetonitrile (MeCN), ethanol (EtOH) were purchased from J&K Scientific. All chemicals were used as received without further purification.

### Growth of $[Pb(C_{12}H_{24}O_6)Cl]_2[Mn_2Cl_6]$ (PMC) single crystals
In a typical synthesis, $MnCl_2$ (0.1 mmol), $PbCl_2$ (0.1 mmol) and 18-crown-6 (0.1 mmol) were mixed with MeCN (1.5 ml) in 35 ml vessel. After being sonicated for 10 minutes, the mixture solution was sealed and heated at 120 °C for 24 h in a drying oven, and then steadily cooled at a speed of 5 °C/h to room temperature. The as-synthesized pale-yellow crystals were filtered out, washed with ethanol and dried at 50 °C.

### Characterizations
Single crystal X-ray diffraction (SCXRD) data were collected by a Bruker D8 Venture X-ray single crystal diffractometer. Data were measured by using monochromatic Mo Kα radiation. Data reduction, scaling, and absorption corrections were performed by using SAINT (Bruker, V8.38A, 2013). The data were solved with the ShelXT structure solution program by using the Intrinsic Phasing solution method. [1, 2] The model was refined with the ShelXL program using Least-squares minimization method.[3] PXRD patterns were recorded on an X-ray diffractometer (Rigaku SmartLab) with Cu Kα radiation (λ = 0.15418 nm) at a voltage of 45 kV and a current of 200 mA. The photoluminescence (PL) and PL excitation (PLE) spectra were taken by a HORIBA Scientific FluoroMax-4 spectrofluorometer and an Edinburgh FLS1000 fluorescence spectrometer. Temperature-dependent spectra were measured on a HORIBA Scientific FluoroMax-4 spectrofluorometer with a heating apparatus as the heating source. PL lifetime measurements were performed using $\mu$F2 microsecond flash lamp as the excitation source on an Edinburgh FLS1000 fluorescence spectrometer. The PL decay curves of all samples were fitted with

$$\tau_{avg} = (\sum_{i=1}^{n} \tau_i^2 A_i)/(\sum_{i=1}^{n} \tau_i A_i)$$

where $A_i$ and $t_i$ are the corresponding amplitudes and exponential decay parameters in mono-exponential (n = 1) analysis. The absolute photoluminescence quantum yield (PLQY) was determined by using a Teflon-lined integrating sphere accessory into the FLS1000 fluorescence spectrometer. The power-dependent PL emission was monitored by a power meter of Thorlab PM100D with a standard photodiode power sensor (S120VC). Thermogravimetric analysis (TGA) and differential scanning calorimetry (DCS) were performed by heating and cooling the polycrystalline samples on a PerkinElmer Diamond DSC instrument in the temperature range 30 - 1100 K with a heating rate of 20 K·min$^{-1}$ under nitrogen atmosphere. All the photographs were taken on Canon EOS 5D Mark IV with Canon MP-E 65 mm f/2.8 1-5X Macro lens. The white LED was fabricated using a blue InGaN chip (Em = 450 nm, 3 V, Shenzhen Looking Long Technology Co., Ltd, China) and a yellow phosphor PMC, the proper amounts of PMC were thoroughly mixed with epoxy resin, and they were coated on blue chip. The photoelectric properties, including the emission spectra, correlated color temperature (CCT), luminous efficacy, and CIE color coordinates of LED devices were measured by using an integrating sphere spectroradiometer system (HAAS-2000, Everfine).

### Data analyses
*Calculation of two tetrahedral parameters:* the following two parameters are calculated to quantify the magnitude of distortion within a tetrahedral structure.[4]

Tetrahedral bond angle variance:

$$\sigma_{tet}^2 = 1/5\sum_{i=1}^{5}(\Theta_i - 109.47)^2$$

Tetrahedral bond length distortion index:

$$\Delta d_{tet} = 1/4\sum_{i=1}^{4}((d_i - d_0)/d_0)^2$$

where $q_i$ is the bond angle of Cl-Mn-Cl', $d_0$ is the average distance of Mn-Cl bond and $d_i$ is the individual length of Mn-Cl bond.

*Calculation of the activation energy:* the activation energy *ΔE* of PMC was calculated by using the following Arrhenius formula:[5]

$$I_0/I_t = 1 + A * e^{\frac{-\Delta E}{kT}}$$

where $I_0$ and $I_t$ are the emission intensity at 300 K and the experimental temperature, A is a constant, and $k$ is the Boltzmann constant ($k$ = 8.617×10$^{-5}$ eV K$^{-1}$).
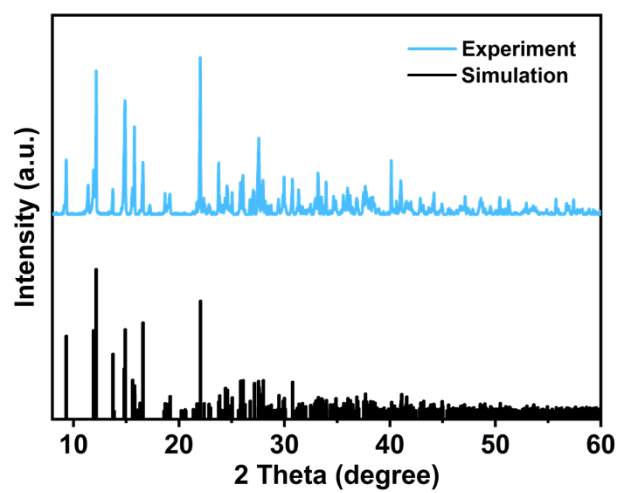
# Results and Discussion



**Fig. S1** Experimental pattern of the powder X-ray diffraction (PXRD) matches well with the simulated one, verifying the purity of PMC.
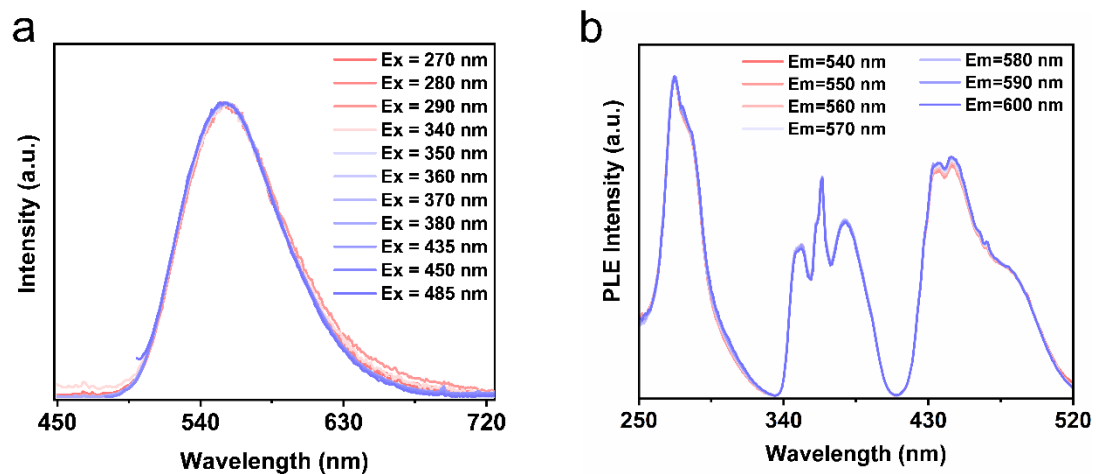
**Fig. S2** (a) Normalized excitation wavelength-dependent PL spectra of PMC crystals at room temperature. (b) Normalized emission wavelength-dependent PLE spectra of PMC at room temperature.
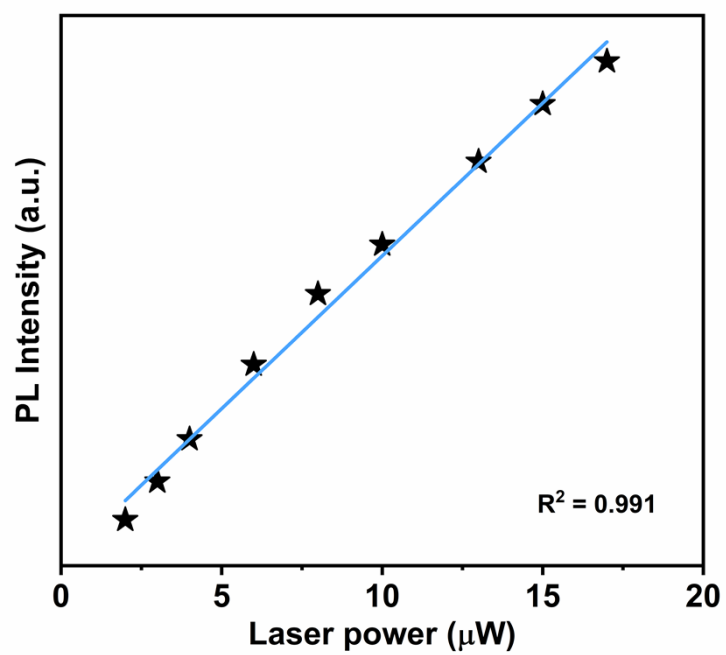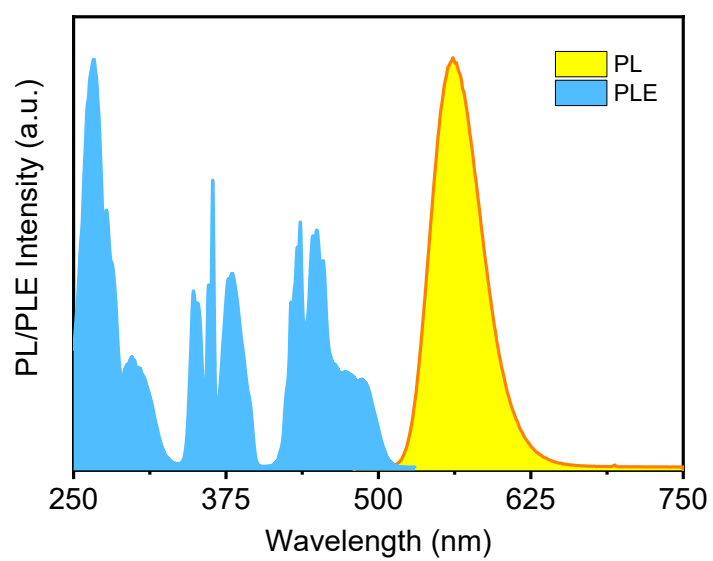
$R^2 = 0.991$

**Fig. S3** The power-dependent PL (laser: Ex =405 nm) intensities of PMC (black stars) and the fitting line (blue line).

**Fig. S4** The normalized PL (Ex = 445 nm) and excitation (Em = 556 nm) spectra of PMC at 80 K.
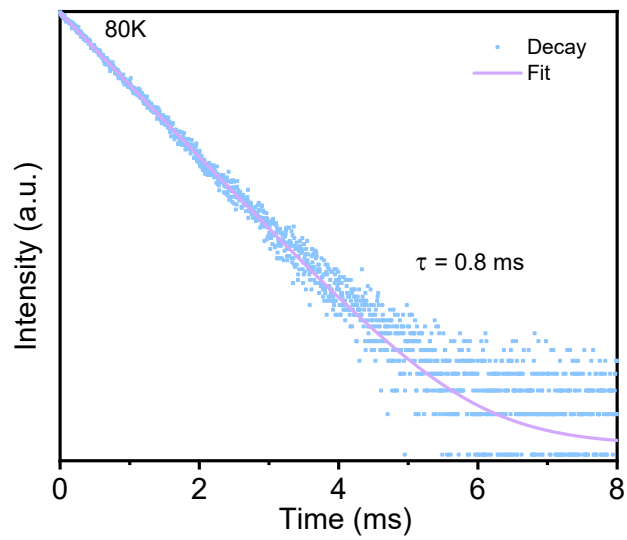
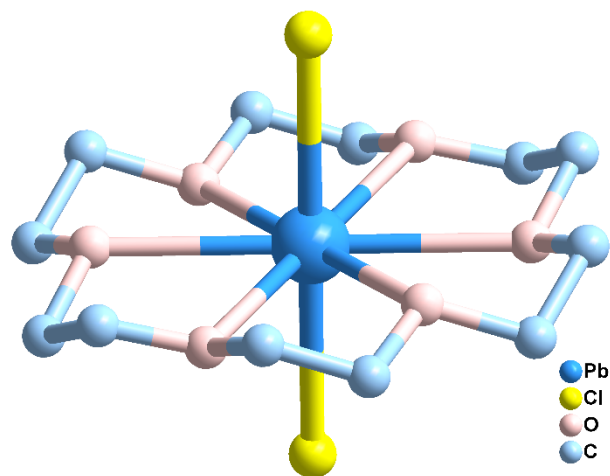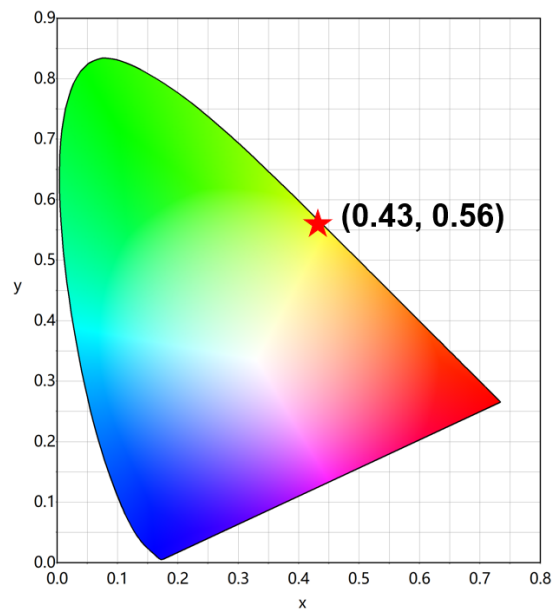**Fig. S5** TRPL decay curve of PMC monitored at 556 nm under 445 nm excitation at 80 K.
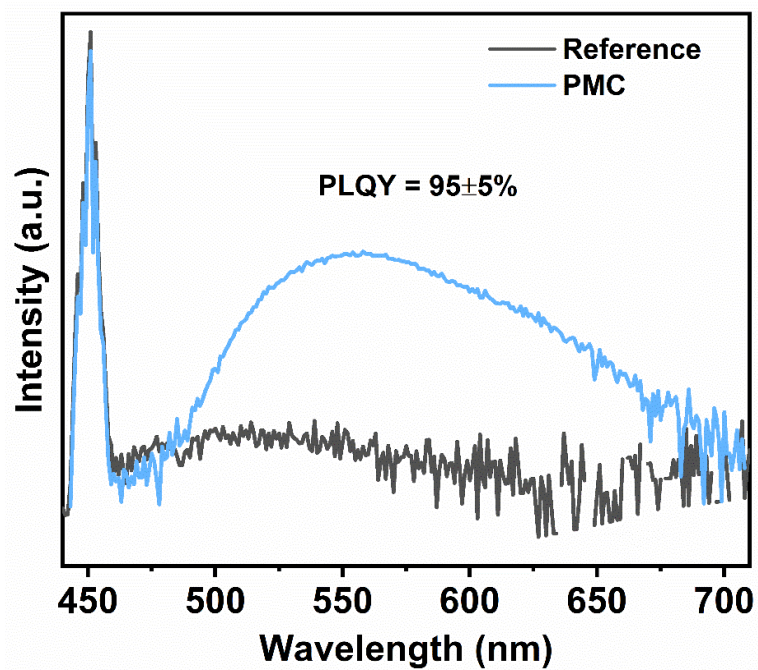
**Fig. S6** Crystal structure of PC (H atoms omitted for clarity).

(0.43, 0.56)

**Fig. S7** The CIE chromaticity coordinate for the yellow emission of PMC under the excitation of 445 nm.

**Fig. S8** Excitation line of reference and emission spectrum of PMC collected under excitation wavelength of 445 nm, collected by an integrating sphere. The PLQY of PMC was calculated to be 95±5%.
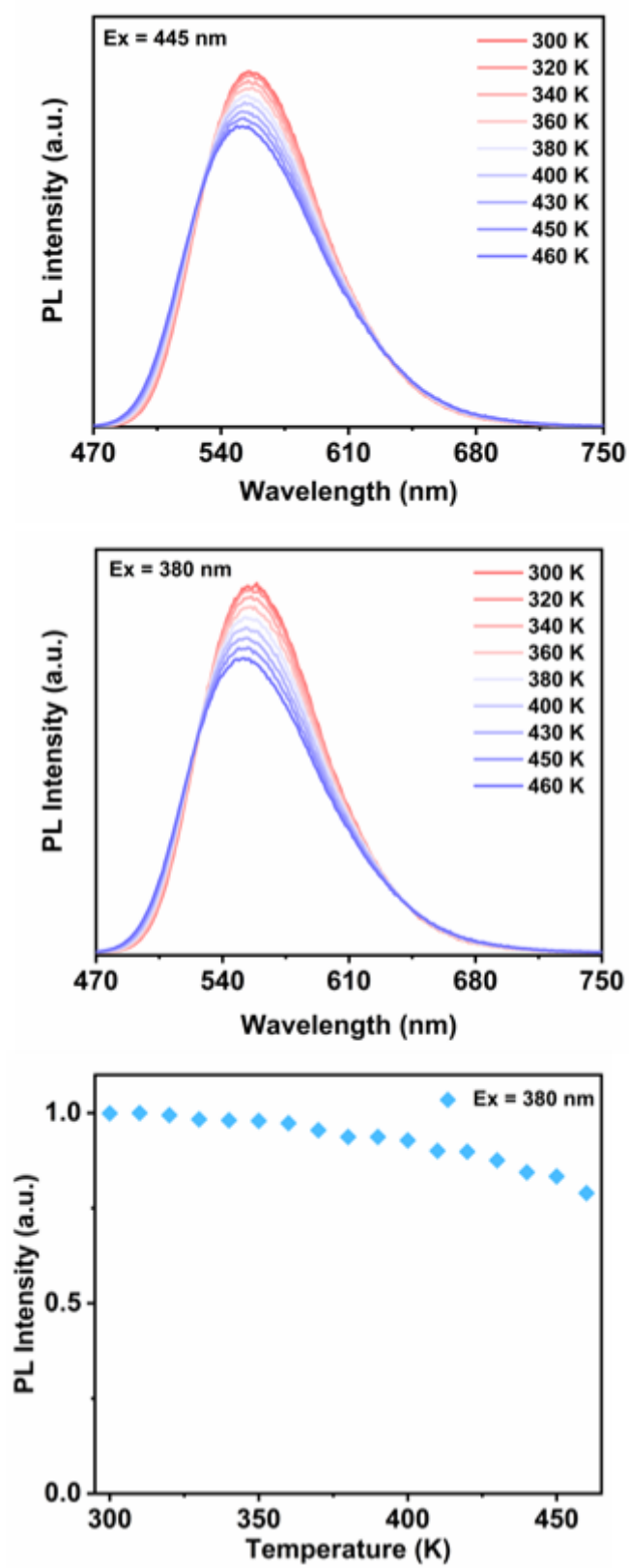
**Fig. S9** Temperature-dependent PL spectra of PMC from 300 to 460 K: (a) Excitation at 445 nm; (b) Excitation at 380 nm. (c) The temperature-dependent normalized PL intensities (Ex = 380 nm) of PMC from 300 K to 500 K.
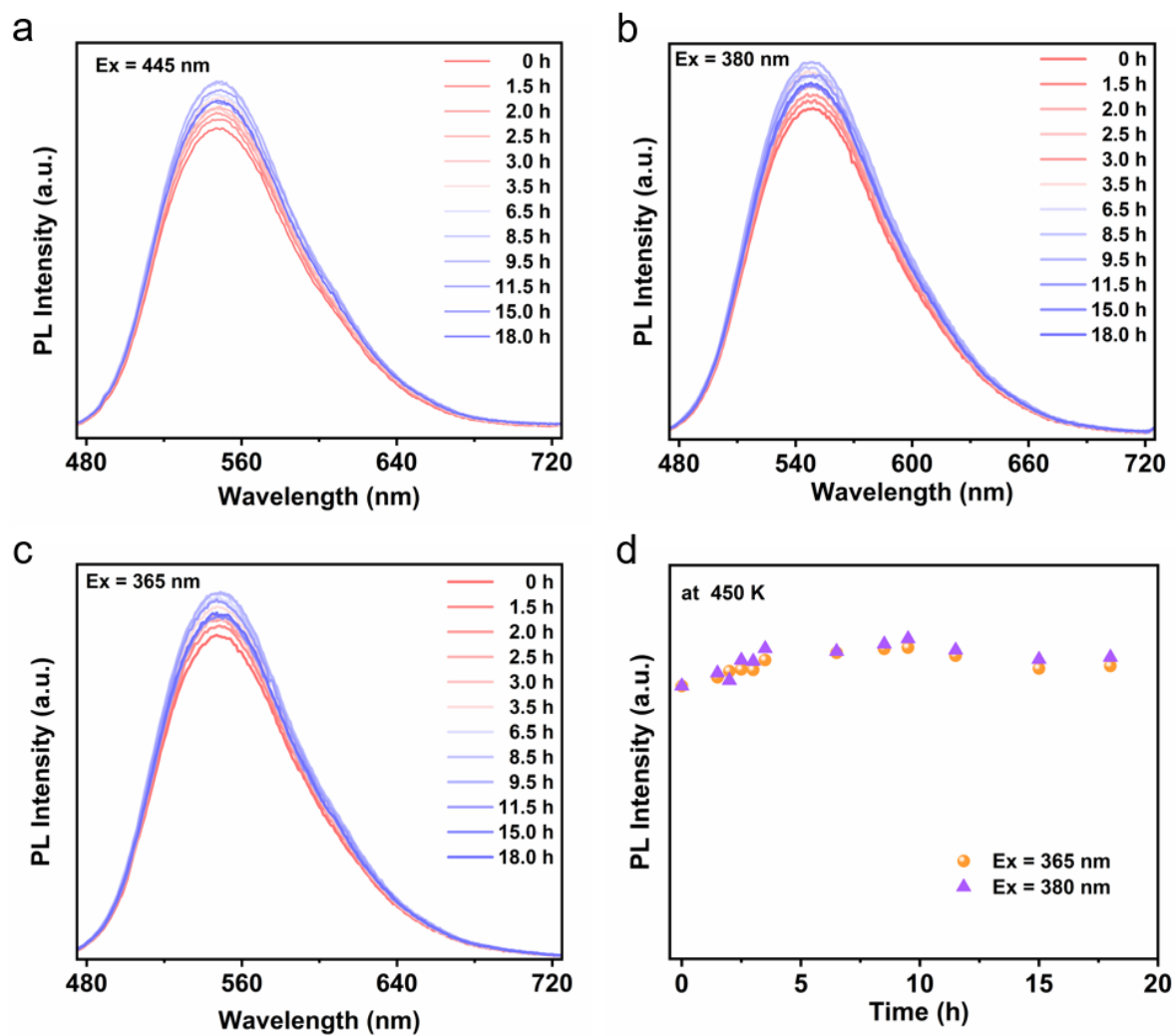
**Fig. S10** Time-dependent PL spectra of PMC at 450 K under various excitation wavelengths: (a) Excitation at 445 nm; (b) Excitation at 380 nm; (c) Excitation at 365 nm. (d) The time-dependent normalized PL intensities (Ex = 365, 380 nm) of PMC at 450 K.
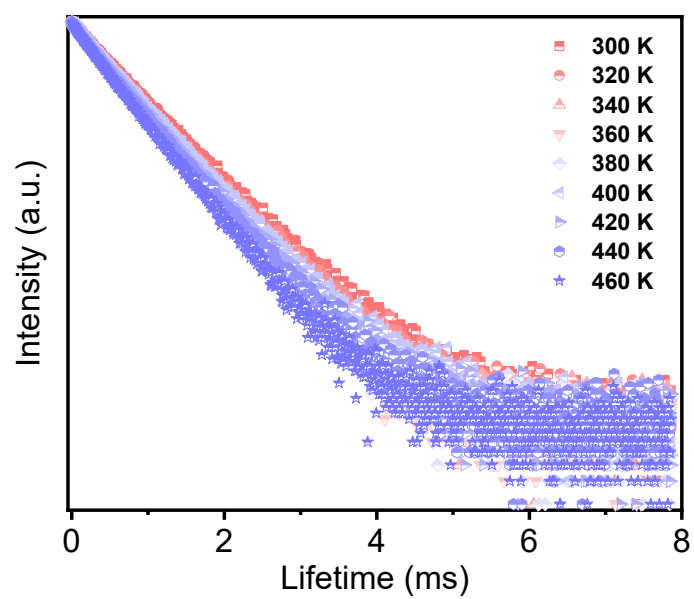
**Fig. S11** TRPL decay curves of PMC monitored at 556 nm under 445 nm excitation under different temperature.
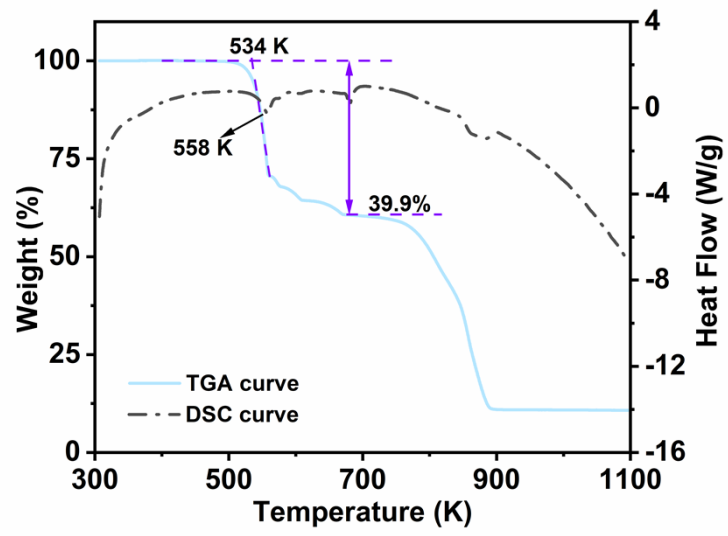
**Fig. S12** The TGA and DSC curves of PMC at the temperature range of 300 - 1100 K.
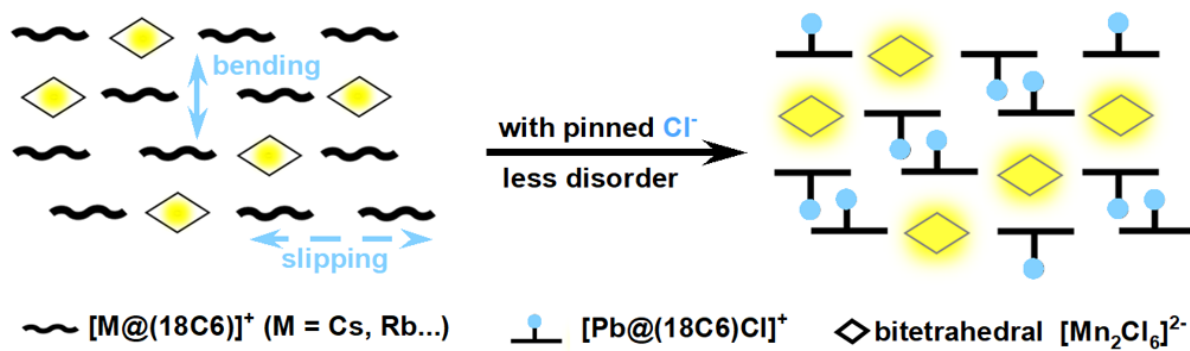
**Fig. S13** Schematic illustrations of the comparison with 18-crown-6-metal systems and pushpin-type cation of PMC (18C8: 18-crown-6).
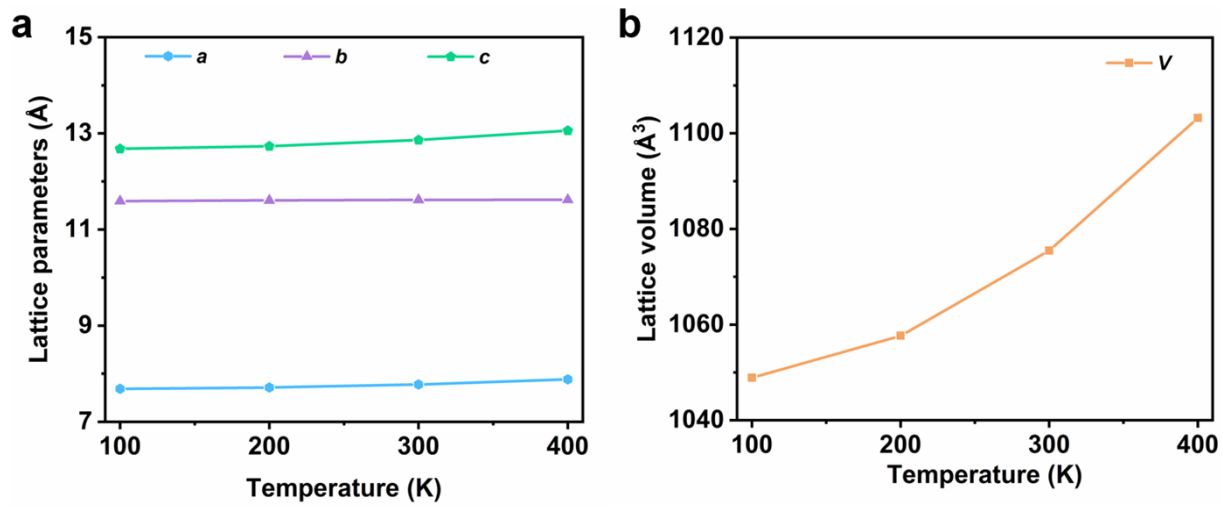
**Fig. S14** (a) The lattice parameters of PMC single crystals under different temperature (100 - 400 K); (b) The lattice volume of PMC single crystals under different temperature (100 – 400 K).
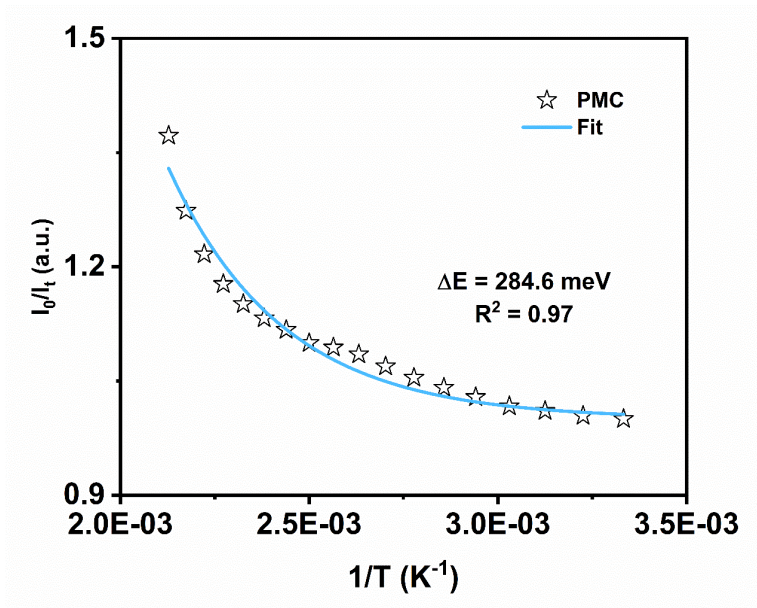
**Fig. S15** The *ΔE* of PMC analyzed by using the Arrhenius equation.
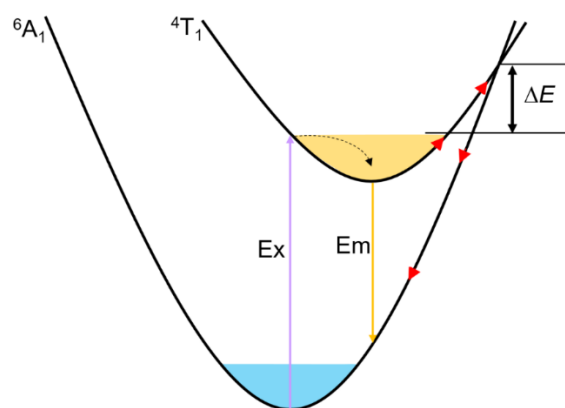
**Fig. S16** Configurational coordination diagram of $Mn^{2+}$ emission: radiative pathway (yellow line); nonradiative pathway (red line); Ex: excitation; Em: emission. $\Delta E$: the activation energy.
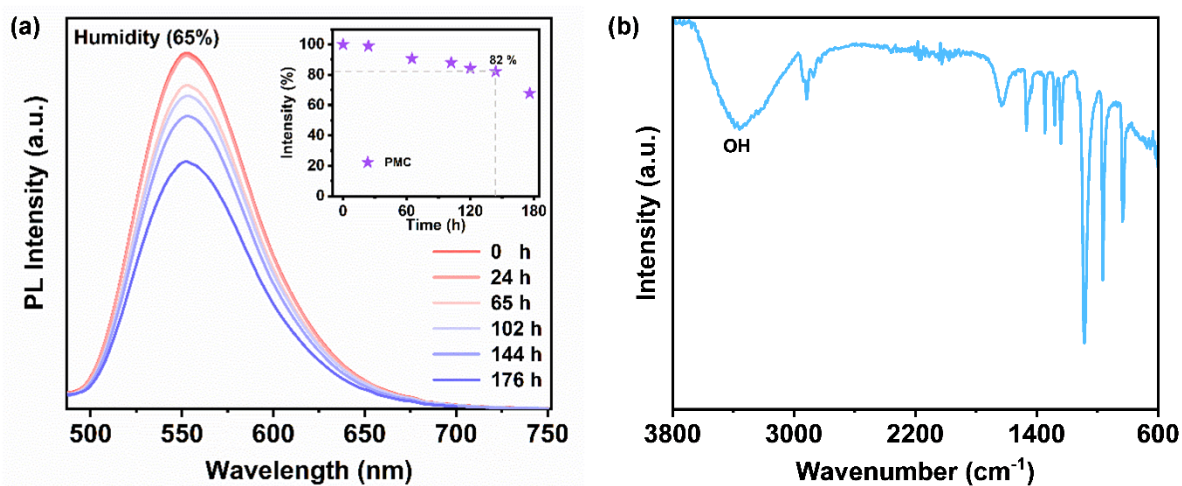
**Fig. S17** (a) Time-dependent PL spectra of PMC exposed to 65% humidity environment under 450 nm excitation, and the inset is the variation of emission intensity over time. (b) The infrared spectrum of PMC exposed in the air with 80% humidity for 3 days. The OH stretching of water centered at 3360 cm$^{-1}$ is observed in the infrared spectrum.
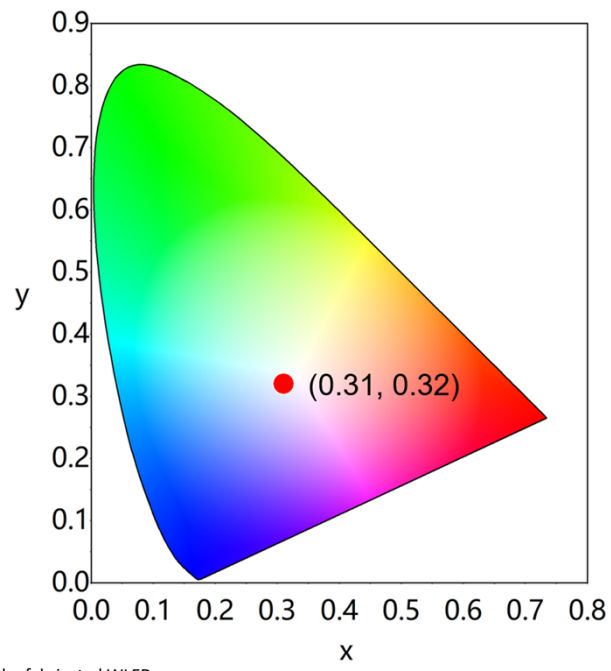
**Fig. S18** The chromaticity coordinate of the fabricated WLED.

**Table S1.** Crystal data and structure refinement for [Pb(C$_{12}$H$_{24}$O$_6$)Cl]$_2$[Mn$_2$Cl$_6$] (PMC).

| Empirical formula | C$_{12}$H$_{24}$Cl$_4$MnO$_6$Pb |
|---|---|
| Formula weight | 668.24 |
| Temperature/K | 100.01 |
| Crystal system | triclinic |
| Space group | *P-1* |
| a/Å | 7.6866(15) |
| b/Å | 11.591(3) |
| c/Å | 12.678(3) |
| α/° | 104.739(7) |
| β/° | 105.642(6) |
| γ/° | 90.148(7) |
| Volume/Å$^3$ | 1048.9(4) |
| Z | 2 |
| $\rho_{calc}$ g/cm$^3$ | 2.116 |
| μ/mm$^{-1}$ | 9.149 |
| F(000) | 638.0 |
| Crystal size/mm$^3$ | 0.15 × 0.1 × 0.1 |
| Radiation | MoKα (λ = 0.71073) |
| 2Θ range for data collection/° | 4.31 to 55.662 |
| Index ranges | -10 ≤ h ≤ 10, -15 ≤ k ≤ 15, -16 ≤ l ≤ 16 |
| Reflections collected | 13799 |
| Independent reflections | 4890 [R$_{int}$ = 0.0661, R$_{sigma}$ = 0.0706] |
| Data/restraints/parameters | 4890/0/217 |
| Goodness-of-fit on $F^2$ | 1.064 |
| Final R indexes [I>=2σ (I)] | R$_1$ = 0.0355[a], wR$_2$ = 0.0849[b] |
| Final R indexes [all data] | R$_1$ = 0.0441[a], wR$_2$ = 0.0885[b] |
| Largest diff. peak/hole / e Å$^{-3}$ | 1.57/-2.18 |

[a] $R_1 = \Sigma |F_o - F_c| / \Sigma F_o$     [b] $wR_2 = \Sigma[w(F_o^2 - F_c^2)^2] / \Sigma[w(F_o^2)]^{1/2}$

**Table S2.** Selected bond distances of PMC at 100 K.

| Bond | Length (Å) | Bond angle | Angle (°) |
|---|---|---|---|
| Pb1-Cl4 | 2.543(14) | Cl1-Mn-Cl1[1] | 92.23 (5) |
| Pb1-Cl3 | 3.319(7) | Cl2-Mn-Cl1 | 110.65(6) |
| Pb1-O1 | 2.662(4) | Cl2-Mn-Cl1[1] | 113.04(6) |
| Pb1-O2 | 2.754(4) | Cl2-Mn-Cl3 | 114.78(6) |
| Pb1-O3 | 2.809(4) | Cl3-Mn-Cl1[1] | 107.45(6) |
| Pb1-O4 | 2.800(4) | Cl3-Mn-Cl1 | 116.53(6) |
| Pb1-O5 | 2.756(4) | / | / |
| Pb1-O6 | 2.692(4) | / | / |
| Mn1-Cl1 | 2.4368(17) | / | / |
| Mn1-Cl1[1] | 2.4390(16) | / | / |
| Mn1-Cl2 | 2.3075(17) | / | / |
| Mn1-Cl3 | 2.3305(16) | / | / |

23

**Table S3.** The comparison of the structural distortion of PMC and reported Mn halides.

| Materials | $\lambda_{em}$ | $\sigma_{tet}^2$ | $\Delta d_{tet}$ | References |
|---|---|---|---|---|
| $(Ph_4P)_2MnCl_4$ | 517 | 4.9 | $3.80*10\text{^}-7$ | [6] |
| $Bz(Me)_3NMnCl_4$ | 547 | 39.0 | $1.04*10\text{^}-4$ | [7] |
| $Bmpip_2MnCl_4$ | 513 | 6.6 | $1.05*10\text{^}-5$ | [7] |
| $(KC)_2MnCl_4$ | 518 | 7.5 | $7.63*10\text{^}-5$ | [8] |
| $Py_2MnCl_4$ | 518 | 6.8 | $8.49*10\text{^}-6$ | [9] |
| $C_{11}N_2H_{22}MnCl_4$ | 530 | 14.4 | $2.25*10\text{^}-5$ | [10] |
| $(C_4NOH_{10})_2MnCl_4$ | 520 | 25.7 | $1.02*10\text{^}-4$ | [11] |
| $EtMe_3NMnCl_4$ | 525 | 1.3 | $7.97*10\text{^}-6$ | [12] |
| **PMC** | **556** | **78.7** | **$7.08*10\text{^}-4$** | **This work** |

**Table S4.** The comparison of different representative yellow-emissive materials.

| Materials | | $l_{Em}$ (nm) | Temp.(K) | Ratio to Intensity@ RT (%) | RT PLQY (%) | Ref. |
|---|---|---|---|---|---|---|
| | PMC | 556 | 450 | 90 | 95±5 | This work |
| | $(C_4N_2H_{14}Br)_4SnBr_6$ | 570 | 353 | >90 | 95±5 | [13] |
| | $[Bmim]_2SbCl_5$ | 583 | 349 | <80 | 86.3 | [14] |
| | $(C_4N_2H_{14}Br)_4SnBr_3I_3$ | 582 | 353 | ~50 | ~85 | [15] |
| Hybrid metal halides | $(bmpy)_9[ZnBr_4[Pb_3Br_{11}]$ | 565 | 375 | 78 | 49.8 | [16] |
| | $(TEBA)_2SbCl_5$ | 590 | 375 | 92 | 98 | [17] |
| | $(HMTA)_3Pb_2Br_7$ | 580 | / | <50 | 7 | [18] |
| | $TMEDAPb_2Br_6$ | 554 | / | <50 | 10 | [19] |
| | $HMD_3SnBr_8$ | 600 | / | / | 86 | [20 |
| | $Cs_2Sn_{0.89}Te_{0.11}Cl_6$ | 580 | 323 | <50 | 95.4 | [21] |
| Inorganic metal halides | $Rb_7Sb_3Cl_{16}$ | 560 | / | <50 | 3.8 | [22] |
| | $CsCu_2I_3$ | 568 | / | / | 15.7 | [23] |
| | $Cs_2(Ag_{0.6}Na_{0.4})InCl_6$ | ~560 | 393 | >90 | 86 ± 5 | [24] |
| MOFs | $Zn_6(btc)_4(tppe)_2(DMA)_2$ | 540 | 430 | 94 | 90.7 | [25] |

**Table S5.** Selected bond distances of PMC at different temperature.

| Bond | Length (Å) | | | |
|---|---|---|---|---|
| | 100 K | 200 K | 300 K | 400 K |
| Pb1-Cl4 | 2.543(14) | 2.542(11) | 2.542(14) | 2.540(4) |
| Pb1-O1 | 2.662(4) | 2.689(3) | 2.663(4) | 2.681(12) |
| Pb1-O2 | 2.754(4) | 2.660(3) | 2.685(4) | 2.692(14) |
| Pb1-O3 | 2.809(4) | 2.755(3) | 2.745(5) | 2.738(13) |
| Pb1-O4 | 2.800(4) | 2.811(3) | 2.791(5) | 2.791(11) |
| Pb1-O5 | 2.756(4) | 2.795(3) | 2.807(4) | 2.814(13) |
| Pb1-O6 | 2.692(4) | 2.757(3) | 2.754(4) | 2.762(13) |
| Mn1-Cl1 | 2.4368(17) | 2.4387(14) | 2.4424(17) | 2.454(5) |
| Mn1-Cl1[1] | 2.4390(16) | 2.4409(14) | 2.4423(17) | 2.451(5) |
| Mn1-Cl2 | 2.3075(17) | 2.3086(15) | 2.307(2) | 2.306(6) |
| Mn1-Cl3 | 2.3305(16) | 2.3300(14) | 2.3249(18) | 2.322(5) |

**Table S6.** Lattice parameters of PMC at different temperature.

| Temp.(K) | $a$ (Å) | $b$ (Å) | $c$ (Å) | V (Å$^3$) |
|---|---|---|---|---|
| 100 | 7.6866(15) | 11.591(3) | 12.678(3) | 1048.9(4) |
| 200 | 7.7138(5) | 11.6050(8) | 12.7334(8) | 1057.69(12) |
| 300 | 7.7768(5) | 11.6166(7) | 12.8625(7) | 1075.48(11) |
| 400 | 7.883(3) | 11.619(5) | 13.058(5) | 1103.2(8) |

**References**

[1]     G. M. Sheldrick, *Acta Cryst.* 2015, **A71**, 3;

[2]     O. V. Dolomanov, L. J. Bourhis, R. J. Gildea, J. A. K. Howard, H. Puschmann, *J. Appl. Cryst.* 2009, **42**, 339.

[3]     A. Linden, *Acta Cryst.* 2015, **C71**, 1.

[4]     K. Robinson, G. V. Gibbs, P. H. Ribbe, *Science* 1971, **172**, 567.

[5]     S. Bhushan, M. V. Chukichev, *J. Mater. Sci. Lett.* 1988, **7**, 319.

[6]     G. Zhou, Z. Liu, M. S. Molokeev, Z. Xiao, Z. Xia, X.-M. Zhang, *J. Mater. Chem. C* 2021, **9**, 2047.

[7]     V. Morad, I. Cherniukh, L. Pottschacher, Y. Shynkarenko, S. Yakunin, M. V. Kovalenko, *Chem. Mater.* 2019, **31**, 10161.

[8]     J. Zhao, T. Zhang, X. Y. Dong, M. E. Sun, C. Zhang, X. Li, Y. S. Zhao, S. Q. Zang, *J. Am. Chem. Soc.* 2019, **141**, 15755.

[9]     C. Li, X. Bai, Y. Guo, B. Zou, *ACS Omega* 2019, **4**, 8039.

[10]    Z. X. Wang, P. F. Li, W. Q. Liao, Y. Tang, H. Y. Ye, Y. Zhang, *Chem. Asian J.* 2016, **11**, 981.

[11]    M. E. Sun, Y. Li, X. Y. Dong, S. Q. Zang, *Chem. Sci.* 2019, **10**, 3836.

[12]    Y. Z. Zhang, D. S. Sun, X. G. Chen, J. X. Gao, X. N. Hua, W. Q. Liao, *Chem. Asian J.* 2019, **14**, 3863.

[13]    M. Worku, Y. Tian, C. Zhou, S. Lee, Q. Meisner, Y. Zhou, B. Ma, *ACS Appl. Mater. Interfaces* 2018, **10**, 30051.

[14]    Z. P. Wang, J. Y. Wang, J. R. Li, M. L. Feng, G. D. Zou, X. Y. Huang, *Chem. Commun.* 2015, **51**, 3094.

[15]    C. Zhou, Y. Tian, Z. Yuan, H. Lin, B. Chen, R. Clark, T. Dilbeck, Y. Zhou, J. Hurley, J. Neu, T. Besara, T. Siegrist, P. Djurovich, B. Ma, *ACS Appl. Mater. Interfaces* 2017, **9**, 44579.

[16]    M. Li, J. Zhou, G. Zhou, M. S. Molokeev, J. Zhao, V. Morad, M. V. Kovalenko, Z. Xia, *Angew. Chem., Int. Ed.* 2019, **58**, 18670.

[17]    Z. Li, Y. Li, P. Liang, T. Zhou, L. Wang, R.-J. Xie, *Chem. Mater.* 2019, **31**, 9363.

[18]    H. Lin, C. Zhou, Y. Tian, T. Besara, J. Neu, T. Siegrist, Y. Zhou, J. Bullock, K. S. Schanze, W. Ming, M.-H. Du, B. Ma, *Chem. Sci.* 2017, **8**, 8400.

[19]    H. Lin, C. Zhou, J. Neu, Y. Zhou, D. Han, S. Chen, M. Worku, M. Chaaban, S. Lee, E. Berkwits, T. Siegrist, M. H. Du, B. Ma, *Adv. Opt. Mater.* 2019, **7**, 1801474.

[20]    P. Fu, M. Huang, Y. Shang, N. Yu, H. L. Zhou, Y. B. Zhang, S. Chen, J. Gong, Z. Ning, *ACS Appl. Mater. Interfaces* 2018, **10**, 34363.

[21]    Z. Tan, Y. Chu, J. Chen, J. Li, G. Ji, G. Niu, L. Gao, Z. Xiao, J. Tang, *Adv. Mater.* 2020, **32**, 2002443.

[22]    B. M. Benin, K. M. McCall, M. Worle, V. Morad, M. Aebli, S. Yakunin, Y. Shynkarenko, M. V. Kovalenko, *Angew. Chem., Int. Ed.* 2020, **59**, 14490.

[23]    R. Lin, Q. Guo, Q. Zhu, Y. Zhu, W. Zheng, F. Huang, *Adv. Mater.* 2019, **31**, 1905079.

[24]    J. Luo, X. Wang, S. Li, J. Liu, Y. Guo, G. Niu, L. Yao, Y. Fu, L. Gao, Q. Dong, C. Zhao, M. Leng, F. Ma, W. Liang, L. Wang, S. Jin, J. Han, L. Zhang, J. Etheridge, J. Wang, Y. Yan, E. H. Sargent, J. Tang, *Nature* 2018, **563**, 541.

[25]    Q. Gong, Z. Hu, B. J. Deibert, T. J. Emge, S. J. Teat, D. Banerjee, B. Mussman, N. D. Rudd, J. Li, *J. Am. Chem. Soc.* 2014, **136**, 16724.